Analysis of bearing capacity of reinforced retaining structures

Jan Derksen & Martin Ziegler
Geotechnical Engineering, RWTH Aachen University, Germany

Oliver Detert & Hartmut Hangen
HUESKER Synthetic GmbH, Germany

ABSTRACT: Retaining structures are one of the commonly used applications of geogrid reinforced soil. Most design codes such as EBGEO, BS8006 and other international regulations assume a multi-body failure mechanism below a quasi-monolithic reinforced block securing adequate bearing capacity for retaining walls. Consequently, the flexible behavior of the geogrid reinforcement is not taken into account. Therefore, laboratory model tests have been developed at the Geotechnical Institute of RWTH Aachen University to investigate the bearing capacity behavior of both rigid and flexible retaining structures. The laboratory model tests illustrate the crucial failure kinematics of reinforced retaining structures qualitatively. A path-controlled punching force is increased on top of the structures until post failure behavior of the specimen is observed. During loading the deformation of the soil is evaluated with the digital image correlation (DIC) method. The results visualize the development of shear bands and indicate different failure modes for rigid and flexible retaining walls. Bearing capacity failure occurred in cases of flexible geogrid reinforced walls, whereas a comparable rigid wall failed by sliding and overturning. Moreover, an improved bearing capacity resistance is observed with enlarged geogrid anchorage length. Based on the experimental results a numerical model is set up in order to investigate the influence of wall geometry, soil and geogrid properties on occurring failure modes. First results confirm the capability of the finite element analysis to simulate the mechanisms observed in the laboratory qualitatively.

Keywords: geogrid, reinforced wall, failure modes, model test, DIC, numerical simulation, hardening soil

1 INTRODUCTION

Retaining structures are one of the commonly used applications of geogrid reinforced soil and require a proof of adequate bearing capacity. The design concepts for flexible reinforced retaining structures assume a multi-body failure mechanism below a quasi-monolithic reinforced block (EBGEO 2010 and BS8006 2010) in analogy to flat foundations. As a result, rigid and geogrid reinforced walls are treated equally. Hence, the influence of the flexible reinforcement above the foundation base is not taken into account. Therefore, a review of the actual bearing capacity mechanism is reasonable in order to understand the effect of reinforcement in practical applications and verify the existing calculation approach to enable a realistic design. Thus, laboratory model tests have been developed at RWTH Aachen University to investigate the bearing capacity behavior of both rigid and flexible retaining structures. The objective of the experimental investigation is to analyze the failure mechanism due to vertical load qualitatively.

Based on the experimental results a numerical model is set up in order to investigate the influence of wall geometry, soil and geogrid properties on occurring failure modes.

2 LABORATORY MODEL TESTS

The laboratory model tests intend to enforce a bearing capacity failure below flexible geogrid reinforced and rigid cantilever retaining walls under well-defined boundary conditions. For this purpose geometrical-

ly scaled 1g experiments are chosen, in which the development of failure kinematic is as free as possible from boundary influences.

2.1 *Model setup and test specimen*

The experimental investigations are carried out in a biaxial compression test apparatus, which allows a horizontal deformation only in the direction perpendicular to the wall axis. Consequently, the state of strain in retaining structures are represented by this plain strain conditions. The test apparatus provides an experimental space of 800 x 1220 x 465 [mm] (H x W x D), in which the retaining walls are installed.

The vertical loading is applied with a path-controlled load (2 mm per minute) on top of the retaining structure until post failure behaviour in the subsoil occurs. The punch load is transferred uniformly by an incompressible pressure cushion providing a homogenous stress distribution (see Figure 1). During the experiment the global stresses and strains were recorded. Moreover, soil deformations and kinematic behaviour are observed through the transparent glass side wall in the cross section of the retaining structure using the Digital Image Correlation (DIC) method.

The retaining structures are installed along the entire depth (465 mm) of the test apparatus with a construction height of 200 mm to ensure plane strain conditions. The dimensions of the test specimens are given in Figure 1.

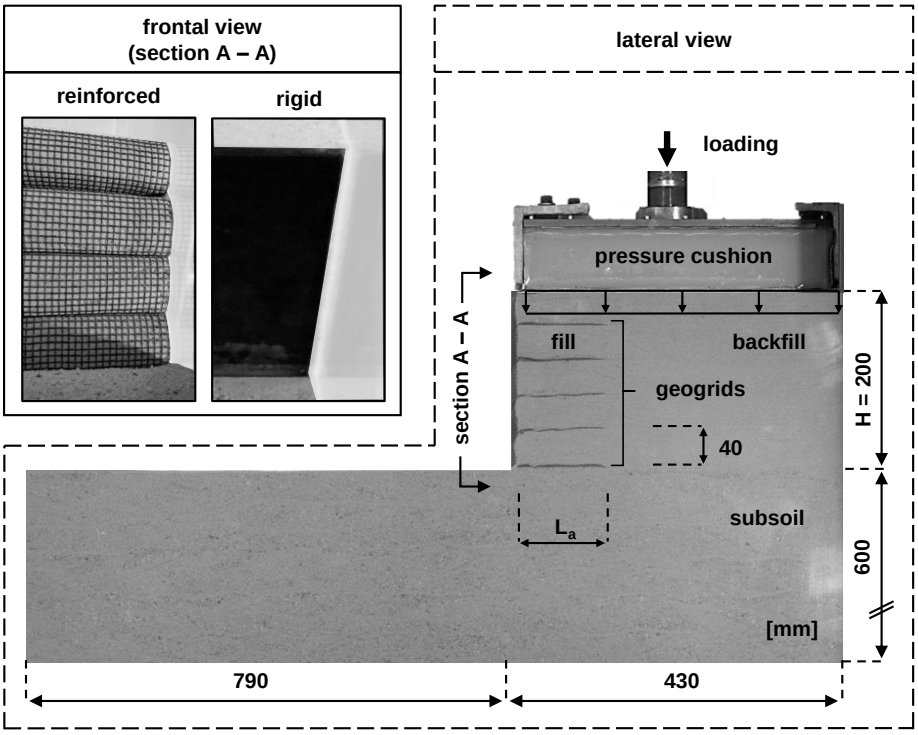

Figure 1. Model setup and test specimen

Figure 2 summarizes the testing program of both rigid and flexible retaining structures, which has been investigated in the present study.

The reinforced walls differ in geogrid anchoring length to construction height ratios $L_a/H = \{0.50; 0.70; 0.85\}$. The median value is chosen according to the EBGEO (2010) recommendation for reinforcement length L_a of 70 % of the construction height H in cases of normal ground conditions and horizontal terrain. The geogrid reinforced walls consist of five reinforcement layers in a vertical distance of 40 mm to each other and a uniform anchoring length L_a. The facing of the wall is constructed with the wrap-around method while a thin nonwoven avoids the sand to run through the geogrid in the front section of the wall.

Tests with a corresponding rigid retaining structure made of steel serve as a reference. Three vertical 2 cm high stripes are installed at the bottom of the horizontal steel plate in order to activate the internal friction angle of the subsoil as contact friction underneath the wall footprint.

A medium sand is chosen for the subsoil, fill and backfill of the retaining walls. According to the Unified Soil Classification System (ASTM D2487) the uniform-graded sand (d_{50} = 0.5 mm) is classified as "SP". The rainfall method was used to prepare the test specimens. The falling height of the sand was varied to prepare different densities in the subsoil (≈ 92 %) and (back-) filling (≈ 99 %) referring to a proctor density of 1.725 g/cm³.

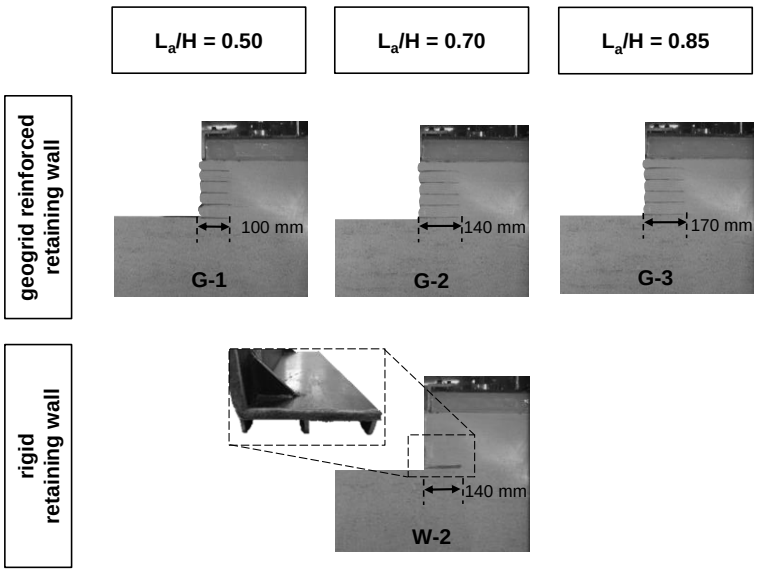

Figure 2. Testing program

The internal peak friction angle of the sand is approximately determined to $\varphi_{0,PS,Dpr\geq 100\%} \approx 60°$ based on comprehensive biaxial compression tests by Ruiken (2013) for the stress range of interest under plain strain conditions. In this case the very high angle of friction occurs due to the nonlinear relationship of shear and normal stresses under low stress states and due to high installation densities ($D_{pr} \geq 100$ %) during the tests. In contrast to that, direct shear tests provide significant lower friction angles for the subsoil $\varphi_{0,DS,Dpr=94\%} \approx 39°$ and the filling $\varphi_{0,DS,Dpr=99\%} \approx 44°$ material considering different installation densities. Results obtained from triaxial compression tests give values for friction angles between those of biaxial compression and direct shear tests. Hereby the known constraint of the friction angle on the test boundary conditions is confirmed.

The model geogrid used for the reinforced structures is a regular biaxial product made of PET. The tensile strength $F_{max} = 17.3$ kN/m ($\varepsilon_{max} = 16.9$ %) and tensile stiffness $J_{0\text{-}2\%} \approx 150$ kN/m are obtained from laboratory tensile tests. The geometry of the grid can be described by an opening size of $d_{o1} \approx d_{o2} \approx 3$ mm and a thickness of 0.81 mm.

Moreover, the contact friction angle between soil and model geogrid is determined to be approximately the friction angle of the soil based on direct shear tests. The influence of the glass wall due to friction can be neglected in accordance to Tatsuoka and Haibara (1985) as the contact friction angle between glass and sand is evaluated to be less than 7°.

2.2 *Experimental results*

The intention of the laboratory model test is to visualize the failure kinematics of loaded retaining walls. The particle displacements and rotations are evaluated by sequential taken pictures during vertical loading using the DIC method (Raffel et al. 2007). The displacement field of the soil particles is calculated by comparing image patterns in different deformation states, from which the overall displacement and strains of the test specimens are derived. The total displacement of soil represents the deformation of the structure, while particle rotation illustrates failure kinematics. The particle rotation describes changes in direction of the displacement vectors and visualizes the development of shear bands (Bachmann 2008). In this paper vertical strain is defined as ratio of vertical deformations Δs to construction height H of the wall $\varepsilon_v = \Delta s/H$. Similarly, the horizontal strain ε_h is referred to the reinforcement length L_a.

First, effects of anchoring length on bearing capacity resistance will be shown. Then differences between rigid and flexible retaining structures regarding crucial failure mechanisms will be discussed. In addition, a comparison of load capacities of the structures is possible due to the recorded vertical loading and deformation.

2.2.1 *Anchoring length*

Figure 3 compares particle rotations of three geogrid reinforced retaining walls, which only differ in anchoring length. Test specimen G-1 with an anchoring length of 100 mm shows a pull-out of the upper reinforcement layer. Due to the difference in stiffness at the transition zone of geogrid reinforcement to

backfill material a settling trough is created, where a horizontal force component cause the squeezing out of the upper geogrid.

In contrast to that, an increase in reinforcement length results in a change in failure mode from pull-out to bearing capacity failure. Furthermore, a significant improved bearing capacity and deformability of reinforced walls is observed with increasing geogrid length, which is visualized by an enlarged shear zone.

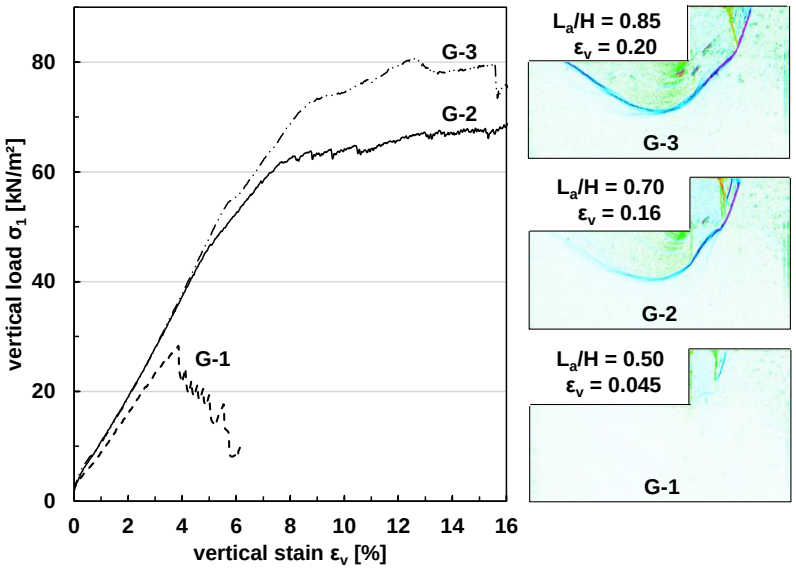

Figure 3. Vertical load capacity and shear bands of geogrid reinforced walls

2.2.2 *Rigid and geogrid reinforced retaining structures*

The kinematic behaviour of rigid and flexible retaining structures ($L_a/H = 0.70$) are compared in Figure 4. Comparing initial and final deformation state ($\varepsilon_v = 0.08$) of the cantilever retaining wall, the failure mechanism of the system is characterized by a slide and overturn movement, which is confirmed by the bending of shear bands towards the horizontal direction underneath the footprint of the wall.

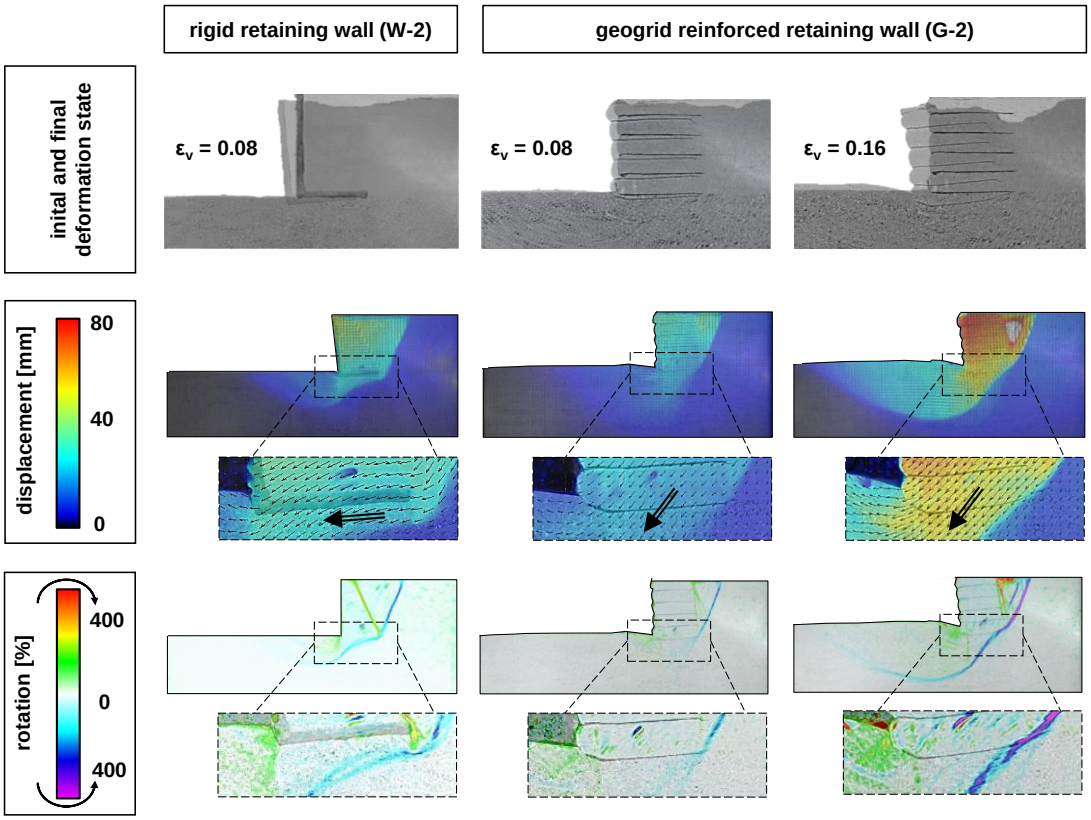

Figure 4. Kinematic behavior of cantilever (W-2) and reinforced (G-2) retaining structures

In contrast, the corresponding geogrid reinforced structure leads to bearing capacity failure in combination with general failure in the final deformation state ($\varepsilon_v = 0.16$). Hereby, shear bands underneath the bottom reinforcement layer are tilted from the horizontal. The failure kinematic of the flexible wall begins at the end of the monolithic reinforced block and leads to a shape similar to common bearing capacity failure in the subsoil. Additionally, the pictures indicate a curved geometrical shape of the lowest geogrid and thus a flexible behaviour of the foundation element.

The overturning mechanism is apparently not decisive for the flexible structure due to the capability of the reinforced block to activate internal resistance in analogy to a cofferdam. Moreover, the flexibility of the reinforcement provides a greater sliding resistance. As a result, the geogrid reinforced wall is able to avoid overturning as well as sliding and shows a failure mode similar to bearing capacity instead.

Whereas the test specimen of the rigid wall shows triangular-shaped failure bodies in the filling material and parallel shear bands to the footprint indicating sliding failure. Accordingly, a dependence of crucial failure mechanism on the construction type of retaining walls can be observed.

The difference in failure mechanisms results in a difference of load capacities of the systems being investigated. First results indicate an around 2 times greater bearing capacity and general stability of the reinforced wall with respect to the sliding and overturning resistance of the cantilever wall (Figure 5). Latter shows 2.5 times larger horizontal displacements than the reinforced wall under equal load due to the mode of failure.

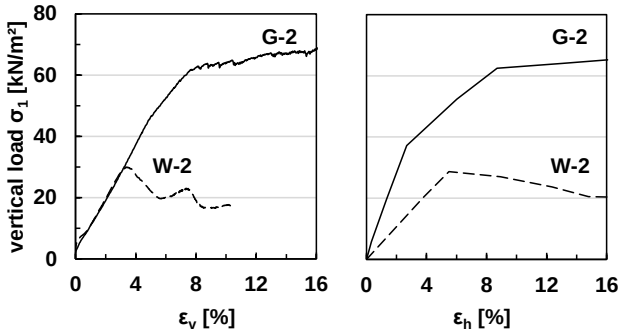

Figure 5. Vertical load capacity and shear bands of geogrid reinforced walls

2.2.3 *Scale effects*

In particular physical model tests are capable for describing mechanical failure mechanisms qualitatively. But a similarity of scaled laboratory model tests to a natural prototype is only given in case of complete mechanical similarity. Otherwise scale effects must be considered, when results of model tests are transferred to large scale problems. In the model tests of the present study scale effects are expected due to the influence of the reduced stress level on the friction angle and the excessive stiffness of the geogrid. As the stiffness of the model geogrid was chosen relatively too high, the wall even behaves much stiffer than a well scaled geogrid. Therefore, the results described will become more distinct in reality.

3 NUMERICAL MODEL SIMULATIONS

The experimental data of the laboratory model tests serve as a basis to set up a finite element model in Plaxis 2D 2017. The general objective of the numerical simulations is to analyze occurring failure modes of the retaining structures for different soil, geogrid parameters and wall geometries. The first approach of the numerical simulations shown in this paper covers the failure kinematics of both rigid and reinforced retaining walls in comparison to the laboratory model tests.

3.1 *Finite element model setup*

The geometry of the numerical model was chosen according to the dimensions of the test apparatus in the laboratory (see Figure 1). Due to the plain strain conditions of the experimental test box a two-dimensional numerical model was set up. The edges of the test apparatus were considered with appropriate contact friction boundary interfaces.

The reinforced wall is constructed layer by layer with corresponding compression phases of each wrapped layer after initial conditions of the subsoil were reached by K_0 procedure. The shape of the geogrid wrap around revetment face was discretized by a rounding off radius to enable a realistic flow of

forces in the reinforcement according to the laboratory test setup. The interaction between geogrid and surrounding soil is modelled with zero thickness interface elements on both sides.

In general, the analysis of deformations requires the application of advanced constitutive models due to non-linear behavior of soil properties. Therefore, the soil behavior was modelled with the Hardening Soil (HS) model according to Schanz et al. (1999). This elastic-plastic constitutive model includes isotropic hardening, stress-dependent stiffness (virgin and un-/reloading), nonlinear elastic stress-strain relationship, dilatancy as well as a multi-surface yield criterion and the Mohr Coulomb failure criterion.

Table 1 summarizes the HS model parameters of the subsoil, filling and backfill material according to different densities obtained by laboratory standard tests.

Table 1. Material properties for the HS constitutive model

parameter	unit	soil	
		subsoil	(back-)fill
γ	kN/m³	15.9	16.8
e_{init}	-	0.68	0.50
e_{min};e_{max}	-	0.482; 0.842	
E_{50}^{ref}	kN/m²	3000	8700
E_{oed}^{ref}	kN/m²	2400	7000
E_{ur}^{ref}	kN/m²	11000	26000
m	-	0.515	0.375
p_{ref}	kN/m²	2.5	
φ	°	41	46
c	kN/m²	2	2
ψ	°	11	14
K_0	-	0.344	0.281
R_f	-	0.5	
R_{inter}	-	1.0	

As a first step, a mesh convergence study was carried out to secure an adequate spatial discretization. Hereby, a four times refined 15-node triangular element mesh (4474 elements) results in a consistent model, that gives no more accurate simulation results with further mesh refinement.

3.2 *Simulation results*

A load was applied by an increasing uniform vertical stress on top of both rigid and reinforced retaining walls until the soil body collapsed. Afterwards the simulation results were analyzed qualitatively with respect to deviatoric strain as an indication for occurring failure kinematics. Figure 6 compares the deviatoric strain of the numerical model simulations to the shear bands observed in the laboratory model tests.

The simulation results of the geogrid reinforced structure confirm the shape of the failure kinematic especially behind and underneath the reinforced monolithic block in accordance with the experimental investigations, in which bearing capacity failure was observed. Furthermore, the allocation of deviatoric strain in case of a rigid retaining wall shows a triangular-shaped soil block in the filling material. The vertical movement of the block causes a shifting of the retaining structure in lateral direction until sliding and overturning failure occurs.

In conclusion, the numerical model simulations indicate the same failure modes that has been observed in the laboratory. Therefore, the numerical simulations confirm the capability of the finite element model to analyze occurring failure kinematics qualitatively. In future studies the numerical model will be used for more extensive investigations regarding crucial failure modes of retaining structures depending on soil and geogrid parameters and wall geometries.

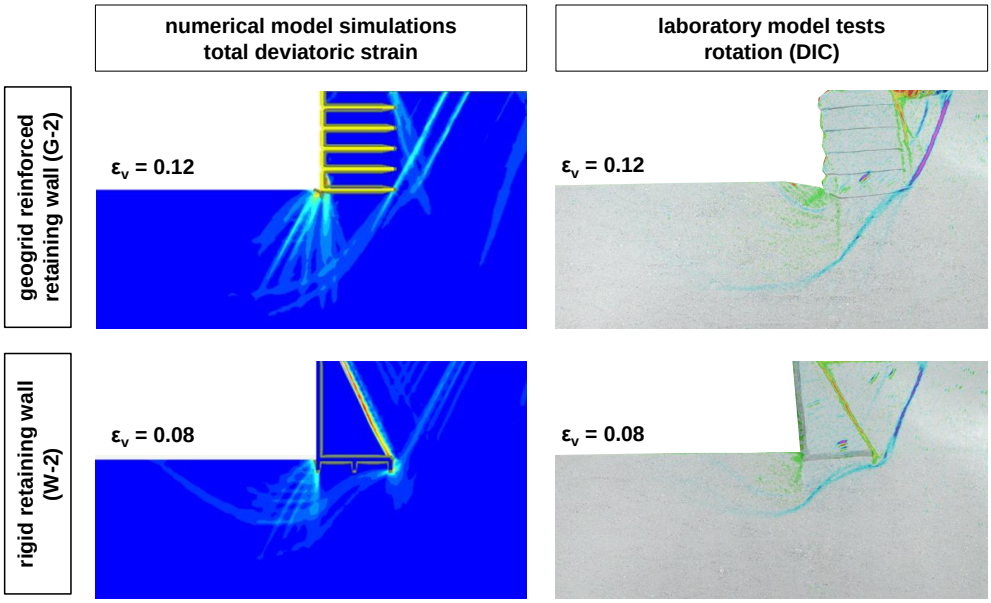

Figure 6. Numerical model simulations (left) and laboratory model tests (right) of both rigid (W-2) and geogrid reinforced (G-2) retaining structures

4 CONCULSIONS

In this paper, laboratory model tests and numerical simulations of both rigid and geogrid reinforced retaining structures were presented.

The experimental test results confirmed a considerable increase in bearing capacity with enlarged reinforcement length resulting in an improved bearing resistance. Moreover, different failure modes were observed for rigid and flexible walls. Bearing capacity failure occurred in cases of flexible geogrid reinforced walls, whereas a comparable rigid wall failed by sliding and overturning. The sliding mechanism was apparently not decisive for reinforced structures due internal resistance and flexibility of the reinforced soil block. Finally, the load resistance of bearing capacity was considerably higher compared to sliding resistance.

First results of numerical simulations with a finite element model confirm the occurring failure kinematics and shear bands qualitatively, which were observed in the laboratory.

REFERENCES

ASTM D 2487. Standard Practice for Classification of Soils for Engineering Purposes (Unified Soil Classification System), American Society for Testing and Materials, West Conshohocken, Pennsylvania, USA.

Bachmann, G. 2008. Progressiver Bruch in Böden – Experimentelle und numerische Untersuchungen, Mitteilungen des Institutes und der Versuchsanstalt für Geotechnik der Technischen Universität Darmstadt, No. 81. Darmstadt, Germany.

BS 8006-1:2010. Code of practice for strengthened/reinforced soils and other fills, BSI British Standards Institution, London, UK.

EBGEO 2010.Recommendations for Design and Analysis of Earth Structures using Geosynthetic Reinforcements – EBGEO, German Geotechnical Society, Ernst & Sohn, Berlin, Germany.

Raffel, M., Willert, C., Wereley, S., Kompenhans, J. 2007. Particle Image Velocimetry – A Practical Guide, Springer Verlag, Berlin, Germany.

Ruiken, A. 2013. Zum Spannungs-Dehnungsverhalten des Verbundbaustoffs « geogitterbewehrter Boden », Lehrstuhl für Geotechnik im Bauwesen der RWTH Aachen, Aachen, Germany.

Schanz, T., Vermeer, P.A., Bonnier, P.G. 1999. The hardening soil model: Formulation and verification. Balkema, Rotterdam, The Netherlands.

Tatsuoka, F. and Haibara, O. 1985. Shear resistance between sand and smooth or lubricated surfaces. Soils and Foundations 25-1 : 89-98.